Enhancement of thermoelectric power factor in $CaGe_2$ films through interlayer atomic modulation

Hu Zhao[1,2], Kenneth Magallon Senados[2], Takeaki Sakurai[2], Takashi Aizawa[1]*, and Takao Mori[1,2]*

1. Research Center for Materials Nanoarchitectonics (MANA), National Institute for Material Science (NIMS), Namiki 1-1, Tsukuba 305-0044, Japan

2. Graduate School of Pure and Applied Sciences, University of Tsukuba, Tennodai 1-1-1, Tsukuba 305-8671, Japan

Authors to whom correspondence should be addressed: AIZAWA.Takashi@nims.go.jp, MORI.Takao@nims.go.jp

Abstract

Group IVA elements Si and Ge and their compounds possess abundant natural distribution and excellent electrical properties that are widely utilized in Si-based technology. The exploration for potentially high-performance thermoelectric materials within the Group IVA elements is a viable pursuit. In this work, Ca intercalated Germanene -$CaGe_2$ films were grown on sapphire substrates by molecular beam epitaxy. It is found that the partial lack of Ca between the germanene buckled layers effectively increases the Seebeck coefficient without restraining the conductivity. A maximum power factor of 170 $\mu W/mK^2$ at 523 K, which is 7 times larger than the stoichiometric $CaGe_2$ film, was achieved in $Ca_{0.835}Ge_2$ film by suppression of bipolar effect and formation of a Ca deficient phase. This study presents a promising approach to tuning the thermoelectric properties of layered semimetal materials through interlayer atomic modulation which induces the buckled structure of the framework layer, thereby modifying the electronic structure.

Thermoelectric generators can convert heat directly into electricity without any chemical reaction or mechanical movement. Thermoelectric generators' high stability and reliability make them perfect candidates for power supply under certain environments [1-3]. Due to the reduced size of integrated circuits, electronic devices are gradually becoming miniaturized. Portable devices are emerging as the mainstream, and implantable devices and sensors are also considered an inevitable trend in development. A chip-sized thermoelectric generator capable of generating microscale energy emerges as a potential power supply for these tiny devices due to its high reliability and security [4-9].

The performance of thermoelectric materials is determined by the figure of merit $ZT= S^2\sigma T/\kappa$, where S is the Seebeck coefficient, σ is the electric conductivity, and κ is the total thermal conductivity [10-12]. The power factor ($S^2\sigma$) is used to measure the electrical performance of thermoelectric materials. Currently, high-performance thermoelectric materials primarily rely on rare and toxic elements like Pb, Bi, and Te, which are harmful to human health, making them unsuitable for applications [13-14]. Group IV-based materials with excellent chemical stability, non-toxicity, and eco-friendly properties can be advantageous for the industry [15]. SiGe alloys have been developed as high-temperature thermoelectric generators by NASA for decades [16]. While the highest ZT value of SiGe alloys was further enhanced to 1.5 at 900 °C, the lower performance around the room temperature range hinders its potential application for powering wearable devices [17-19]. Other silicon-based compounds like higher manganese silicides, CoSi, $FeSi_2$, and $SrSi_2$ have also a lower figure of merit less than 0.1 at room temperature. [19-23].

To achieve high thermoelectric performance at room temperature, a high power factor, and low thermal conductivity are crucial, which presents a significant challenge for semiconductors as the scattering of charge carriers becomes severe due to the high doping impurity concentration [24].

More recently, in addition to metals [25,26], semimetals have emerged as a thermoelectric material that shows a huge power factor at room temperature. The intrinsic high carrier mobility and high band degeneracy in semimetals can lead to a significant leap in the power factor [27,28], for example. Silicene and germanene are well-known two-dimensional electronic materials with exceptionally high carrier mobility [29]. However, their zero bandgap results in a low Seebeck coefficient, similar to that of metals. Many studies have found that intercalating hydrogen atoms or metal atoms into silicene and germanene can distort the two-dimensional lattice, thereby opening a bandgap [30,31]. This phenomenon has already been reported in a silicene-based compound like $CaSi_2$; By altering the position of inserted calcium atoms, a significant power factor was discovered [32,33]. This phenomenon has not yet been observed in germanene-based compounds. However, by adjusting the inserted atoms, a significant improvement in the power factor can be anticipated. In this work, we explored the thermoelectric properties of calcium-intercalated germanene thin films fabricated using molecular beam epitaxy. By adjusting the intercalated calcium atoms and the deposition temperature, we have found that the partial lack of Ca between the germanene buckled layer is effective to increase the Seebeck coefficient without restraining the conductivity, which is attributed to the formation of Ca vacancy and the suppression of the bipolar effect. The addition of Ge second phase further increases the Seebeck coefficient, thus a maximum power factor of 170 $\mu W/mK^2$ at 523 K was achieved in $Ca_{0.835}Ge_2$ film, which is 7 times larger than that of the stoichiometric $CaGe_2$ film.

All $CaGe_2$ films were deposited on a sapphire (0001) substrate using a Molecular beam epitaxy system (EV-500, Eiko). The base pressure in the chamber was 10^{-8} Pa, and the working pressure was maintained in the 10^{-7} Pa range during deposition. Calcium and germanium of 5N purity were placed in separate Knudsen cells and heated to the specified temperatures. In this experiment, the

temperature of the germanium cell ranged from 1150°C to 1200°C, while the temperature of the calcium cell was maintained between 450°C and 500°C. The evaporation rate of each element was determined using a retractable quartz crystal microbalance (QCM) thickness monitor (Q-pod, Inficon), located at the substrate position. The substrate was heated from the back of the sample stage. A thermocouple measured the temperature between the sample holder and the heater, which controled the heater power to keep a specified temperature. The true substrate temperature is considerably lower than the setting temperature denoted as the substrate temperature here. A reflection high-energy electron diffraction (RHEED) was used to monitor the crystallinity of the film surface. The polished sapphire (0001) substrate was immersed in acetone and subjected to ultrasonic cleaning for thirty minutes to remove surface organic containments and dust before being transferred into the vacuum chamber. It was heated to 1000 °C and held for 30 minutes to remove residual impurities then cool down to the deposition temperature. The $CaGe_2$ thin films were obtained by co-depositing calcium and germanium onto the heated sapphire substrate. The deposition time was adjusted to keep all the film thickness around 50 nm.

The phase composition and crystallinity of the films were analyzed by X-ray diffraction (XRD) using a Rigaku MiniFlex X-ray diffractometer with a Cu $K_{\alpha+\beta}$ source (K_α = 1.540593 Å). The surface morphology of films was analyzed using scanning electron microscopy (SEM) (Hitachi High-Tech/S-4800), and the component was analyzed using energy dispersive spectroscopy (EDS) (Hitachi High-Tech/TM-3000). The film thicknesses were measured using a surface profiler system (Bruker Dektak 6M) by step method. Measurements of Hall carrier concentration and Hall mobility at 300 K were performed in a four-probe Hall measurement machine (ResiTest 8300 Hall effect systems). The electric conductivity and Seebeck coefficient of thin films were measured using a ZEM-3 (Advance Riko) apparatus in a He atmosphere.

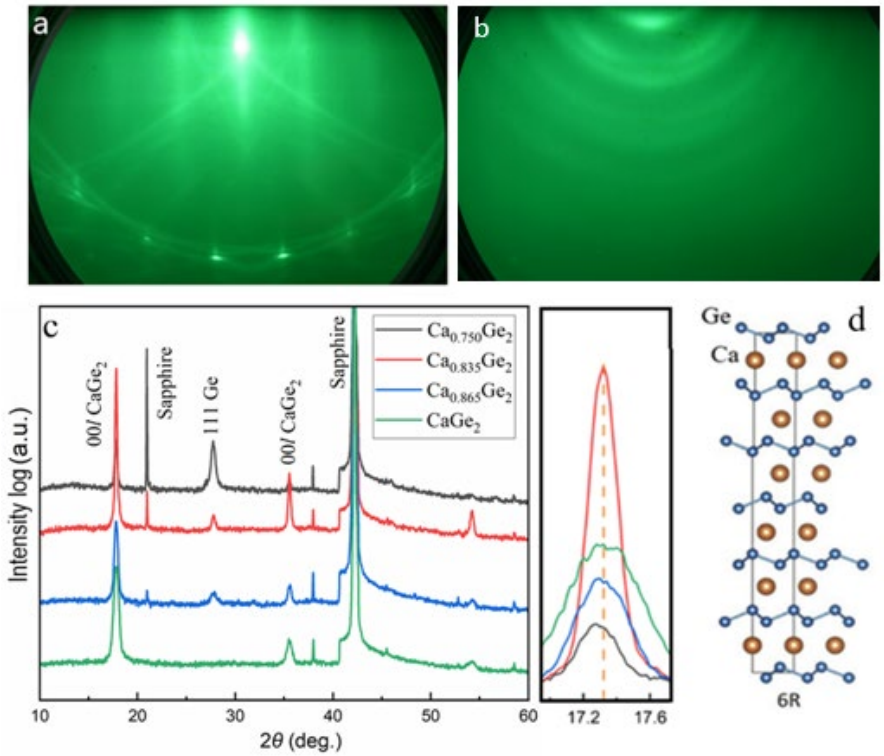

FIG. 1. Diffraction data of Ca_xGe_2 films. (a) RHEED patterns of the Sapphire (0001) surface along $[10\bar{1}0]$. (b) after 30-minute co-deposition of Ca and Ge at 600°C. (c) Log scale θ-2θ X-ray diffraction patterns of Ca_xGe_2 (x = 1, 0.865, 0.835, 0.750) films and linear scale close-up of $CaGe_2$ (006) peak, respectively. (d) Illustration of $CaGe_2$ 6R phase structure.

To investigate the influence of the deformation of the Ge layer on thermoelectric properties, a nonstoichiometric deposition method was used by over-deposition of Ge. By keeping the Ca deposition rate constant and increasing the Ge deposition rate, films with nominal compositions of Ca_xGe_2 (x = 1, 0.865, 0.835, 0.750) were manufactured.

Fig. 1a and b exhibit the respective RHEED patterns of the sapphire (0001) substrate surface showing sharp diffraction spots and Kikuchi lines, and of the co-deposited film of Ca and Ge for 30 minutes at the substrate temperature of 600°C, which shows a multiple ring pattern. The

observed RHEED pattern containing intensity-modulated arcs indicates the polycrystalline film that has a preferred orientation. The multi-ring pattern was still observed even when the substrate temperature increased to 700°C. However, the high dissociation rate of Ca at this temperature led to an uneven film. Conversely, when the temperature was lowered below 500°C, the patterns became cloud-like, indicating the formation of an amorphous structure. This result is consistent with previous reports, where germanium cannot be directly epitaxially deposited on a sapphire (0001) substrate and single-crystal $CaGe_2$ thin films can only be achieved on single-crystal germanium substrates [40]. Unlike homoepitaxial growth on Ge substrates, where surface reconstruction and chemical bonding are favorable, the heteroepitaxial growth on Al_2O_3 is hindered by unfavorable interfacial bonding. Specifically, the bond energy of Ge–O (657.5 ± 4.6 kJ mol^{-1}) is significantly higher than that of Ge–Ge (264.4 ± 6.8 kJ mol^{-1}) [39], which might promote three-dimensional (3D) island growth rather than layer-by-layer monocrystalline growth. In addition, the dissociation of calcium could disrupt the equilibrium conditions required for the epitaxial growth of $CaGe_2$ leading to defect formation, promoting polycrystalline nucleation. Therefore, the polycrystalline Ca_xGe_2 films deposited at 600°C were selected for further research.

TABLE I. The summary of detailed parameters for Ca_xGe_2 films. XRD peak width of the 006 diffraction, calculated lattice constant *c* and calculated grain size, room temperature Hall carrier concentration (*P*) and mobility (μ), and atomic ratio estimated with EDX measurement.

Sample	Atomic ratio Ca/Ge	FWHM deg.	Grain size nm	lattice constant *c* Å	*P* 10^{20} cm^{-3}	μ $cm^2/V/s$
$CaGe_2$	0.5	0.63	12.71	30.77	/	/
$Ca_{0.865}Ge_2$	0.47	0.43	18.68	30.80	7.56	6.05
$Ca_{0.835}Ge_2$	0.44	0.25	32.13	30.84	7.53	11.6

$Ca_{0.75}Ge_2$	/	0.28	28.69	30.89	1.21	0.19

The XRD results of Ca_xGe_2 films are shown in Figure 1c. Two strong peaks located at 17.3°, 35.5°and one weak peak located at 54.2° correspond respectively to the (006), (0012), and (0018) diffractions of the $CaGe_2$ 6R phase, indicating the [001] preferred orientation [37]. The structure of the $CaGe_2$ 6R phase is shown in Figure 1d. Due to the reaction with the intercalated Ca atom, the germanene layer is buckled. The stacking order of the Ge layers here can be described as an *AA′BB′CC′*-like array and repeats every six layers [38]. The additional peak at 27.7° shown in Ca-deficient films corresponds to the Ge (111) peak. The intensity of the Ge peak decreased with the increasing content of Ca indicating the strong correlations between the Ge phase content and Ca composition. The full-width half maximum (FWHM) of the Ca_xGe_2 (006) peak was measured. The smallest FWHM was obtained in $Ca_{0.835}Ge_2$ film around 0.25° while the pristine $CaGe_2$ film has the largest FWHM around 0.6°. Typically, a smaller FWHM indicates higher crystal quality and calcium-deficient films show both superior crystal quality and larger grain sizes compared to stoichiometric films. Moreover, the (006) diffraction peak of $CaGe_2$ appears to shift to slightly lower angles as Ge increases, suggesting the unit cell height c enlargement. As shown in TABLE I, the reduction in calcium content results in an expansion of the *c*. In general, the interlayer atoms in a layered structure are adjustable, and substitution with other atoms or introducing defects often leads to the interlayer spacing variation, thereby affecting the lattice constant [34]. In Ca_xGe_2 film, this lattice parameter expansion may be due to the formation of Ca vacancy since the enlargement is proportional to the amount of the deficiency in Ca content. Unlike usual van der Waals layered crystals, due to the relatively strong interaction between calcium and germanium atoms, the

absence of calcium may influence the electronic and structural arrangement of germanene layers, leading to an expansion of the lattice constant [37].

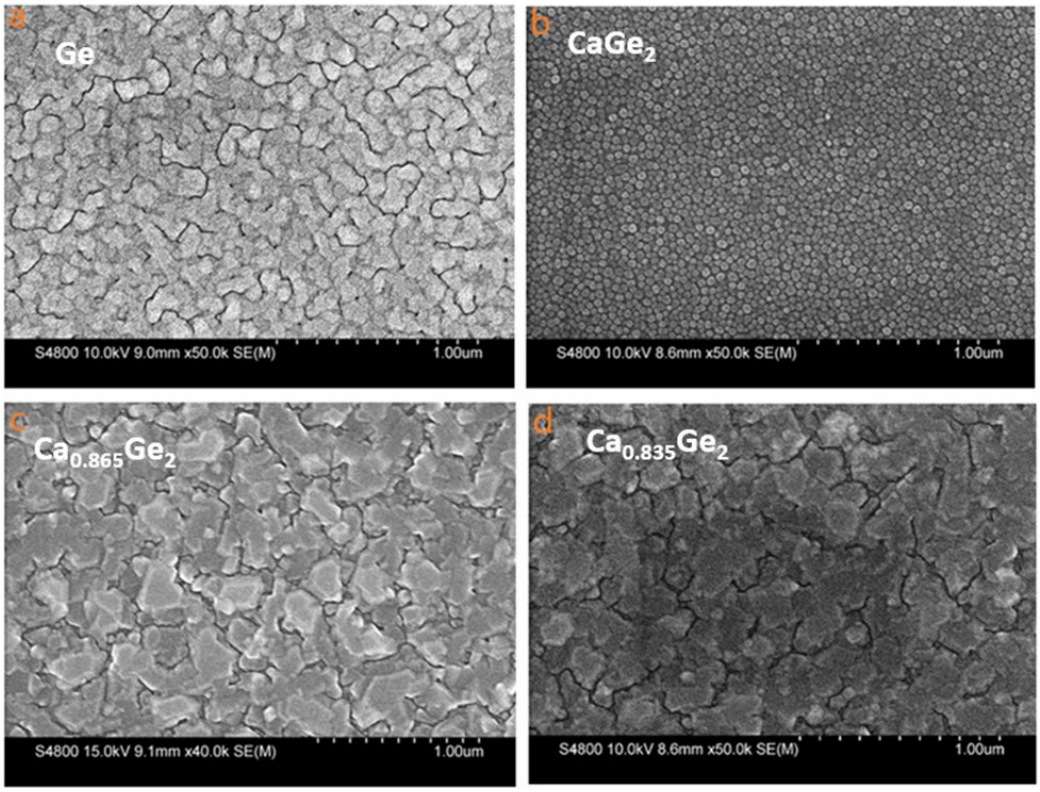

FIG. 2. SEM image of the surface morphology of Ca_xGe_2 films on sapphire substrate. (a) Ge film (b)$CaGe_2$ film (c) $Ca_{0.865}Ge_2$, and (d) $Ca_{0.835}Ge_2$ film.

Fig.2 shows the surface morphology of Ca_xGe_2 (x = 0, 1, 0.865, 0.835) films on sapphire substrates. The variation in calcium content has led to significant differences in the surface morphology of the film. Ge thin films grow via the Volmer-Weber (island-like) mode due to the high lattice mismatch and high interfacial energy between Ge and the sapphire substrate. This three-dimensional growth results in densely packed, distinct crystallites with relatively high surface roughness, which can, in turn, promote crack formation as the film thickness increases. A significant reduction in crystallite size is observed in the case of the stoichiometric $CaGe_2$ thin

film. As shown in Fig. 2(b), the crystallite dimensions are around 30 nm. On the contrary, in the $Ca_{0.865}Ge_2$ and $Ca_{0.835}Ge_2$ samples, enhanced crystallite size has been observed, with some exceeding 300 nm. However, the SEM-observed grain sizes and those calculated from XRD data show noticeable discrepancies. This difference arises because XRD, influenced by the film's preferred orientation, provides the out-of-plane crystallite size, whereas SEM measurements reflect the in-plane grain dimensions. Nonetheless, both methods consistently indicate that Ca deficiency leads to an increase in grain size. This fact indicates that the deficiency of Ca during the film deposition led to an improvement in crystal quality. The substantial difference in crystal quality might be attributed to the quick reaction of Ca and Ge atoms: At 600 ℃, the diffusion of Ge atoms on the substrate surface should be uniform while the quick desorption of unreacted Ca atoms limits the crystal ripening process. In a calcium-deficient environment, Ge atoms could diffuse sufficiently long range and provide more reaction sites for the subsequent Ca atoms, promoting crystal size enlargement. EDS was used to map the elemental distribution of the film and the elemental ratio results are presented in TABLE I. The atomic percentage of Ca in Ca-deficient films is higher than the nominal composition. This deviation may be caused by the inherent instrumental errors and local compositional inhomogeneities.

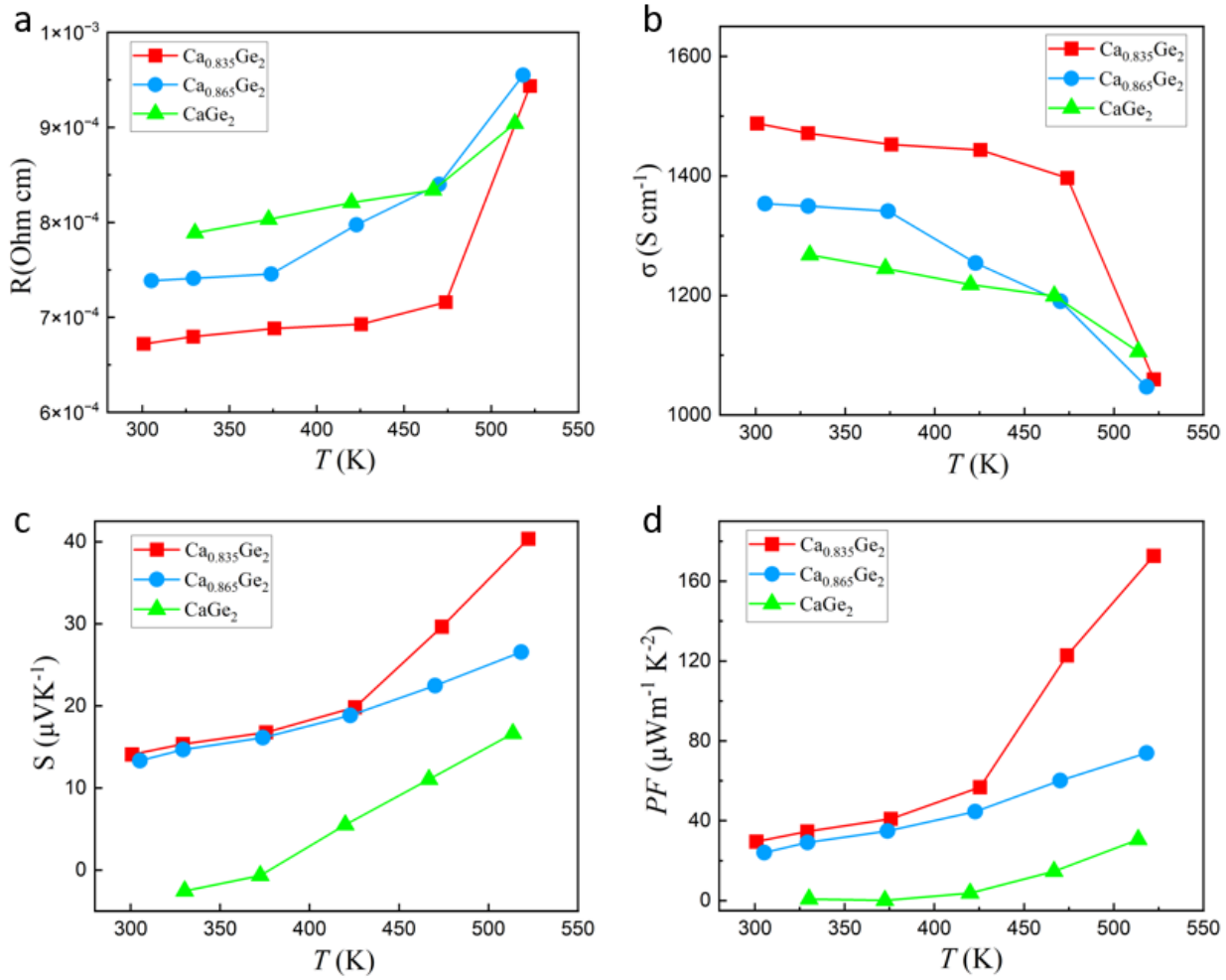

FIG. 3. Temperature-dependent thermoelectric properties of Ca_xGe_2 (x = 1, 0.865, and 0.835) films. (a) resistivity R; (b) electrical conductivity σ; (c) Seebeck coefficient S; (d) power factor PF.

Figure 3 plots the temperature-dependent thermoelectric properties of Ca_xGe_2 (x = 1, 0.865, and 0.835) films. The temperature dependence of electrical conductivity in Fig. 3b exhibits that Ca-deficient films have higher electric conductivity than the pristine film below 450 K. A metallic feature is presented for all films, wherein the conductivity of the sample decreases with an increase in temperature. Conversely in semiconductors, the electrical conductivity tends to increase with a temperature rise. This conductive behavior aligns with the previously reported semi-metallic

properties of the material [40]. The decrease of conductivity with increasing temperature is particularly pronounced in Ca-deficient films. A sharp drop in conductivity was also observed in all films when the temperature exceeded 470K which is significantly influenced by the degree of calcium deficiency. Probably, calcium deficiency may cause increased structural disorder, leading to a sharp decline in conductivity as the temperature rises. Intriguingly, the decrease in electrical conductivity dominated by phonon scattering in metals should follow a trend concerning $T^{-3/2}$, while in this work, the conductivity exhibits a linear relationship within the low-temperature regions. This deviation arises from the intrinsic properties of semimetals, where the carrier concentration increases with temperature due to thermal excitation. The increase in carrier density partially compensates for the reduction in mobility, resulting in a conductivity trend that does not strictly follow the expected $T^{-3/2}$ behavior

As shown in Fig.3c, within the measured temperature range, an increasing positive Seebeck coefficient of the Ca-poor films demonstrates a hole-dominated p-type conduction. Additionally, a transition from negative to positive Seebeck coefficient was observed in the stoichiometric film. This indicates a notable shift in the conductive carrier, transforming from electron-dominant to hole-dominant behavior. In undoped semimetal, the concentration of holes and electrons is almost the same, so that the conductive type is determined by the mobility of electrons and holes [41]. Such a bipolar feature leads to a low Seebeck coefficient in the stoichiometric $CaGe_2$ film. Contrastively, the Ca-poor films showed a higher Seebeck coefficient. In addition, a sharp increase in the Seebeck coefficient above 423 K in the $Ca_{0.835}Ge_2$ sample was observed. As shown in Fig.3d, the power factor of the Ca-poor films is significantly enhanced due to the increase in conductivity and the strengthening of the Seebeck coefficient. Thanks to the remarkable increase in the Seebeck

coefficient at 450 K, a maximum power factor of around 170 $\mu Wm^{-1}K^{-2}$ is achieved in $Ca_{0.835}Ge_2$ film which is 7 times larger than the $CaGe_2$ film.

The measured room temperature Hall carrier concentration and mobility of Ca_xGe_2 films are listed in TABLE I. Due to the strong bipolar effect, the carrier concentration in the stoichiometric sample film could not be measured, while a hole concentration of around $7\square10^{20}$ cm^{-3} was measured in $Ca_{0.835}Ge_2$ and $Ca_{0.865}Ge_2$ film. $Ca_{0.835}Ge_2$ film exhibited the highest mobility among all the samples studied, which resulted in the highest conductivity at room temperature. This enhanced mobility is primarily attributed to its superior crystalline quality, larger grain sizes, and reduced grain boundary scattering. The higher Seebeck coefficient and a stable hole concentration in $Ca_{0.835}Ge_2$ and $Ca_{0.865}Ge_2$ film suggest that calcium deficiency has caused the film's conductivity to transition from metallic to heavily doped p-type semiconductor. Typically, in ambipolar materials, the global Seebeck coefficient can be calculated using the ambipolar Seebeck equation:

$$S = \frac{S_n\sigma_n + S_p\sigma_p}{\sigma_n + \sigma_p}$$

However, in calcium-deficient thin films, the significantly higher electrical conductivity and Seebeck coefficient result in a calculated Seebeck coefficient that is much higher than the measured value. This discrepancy indicates that the bipolar transport behavior observed in $CaGe_2$ thin films does not apply to calcium-deficient films. This finding suggests that the p-type conduction behavior is not merely a consequence of suppressed ambipolar transport due to increased hole concentration but rather originates from the Ca vacancy induced structural modifications.

However, the origin of the anomalous increase of the Seebeck coefficient in $Ca_{0.835}Ge_2$ film above 423 K is still unclear. The effect of the second Ge phase should be considered. In polycrystalline, the energy filtering effect or carrier modulation doping caused by the second phase is often considered as an effective approach to enhancing the Seebeck coefficient [42].

To explore the effect of the Ge second phase on the thermoelectric performance of the film, a controlled experiment was designed to compare the performances of Ge crystal-contained film and Ca-poor film. A hetero-structured $CaGe_2$/Ge/Sapphire was grown as a control. The 10 nm Ge crystal was initially grown on a sapphire substrate, and then a stoichiometric 50 nm $CaGe_2$ film was overlayed on it. The temperature-dependent thermoelectric properties of the hetero-structured film are shown in Fig 4.

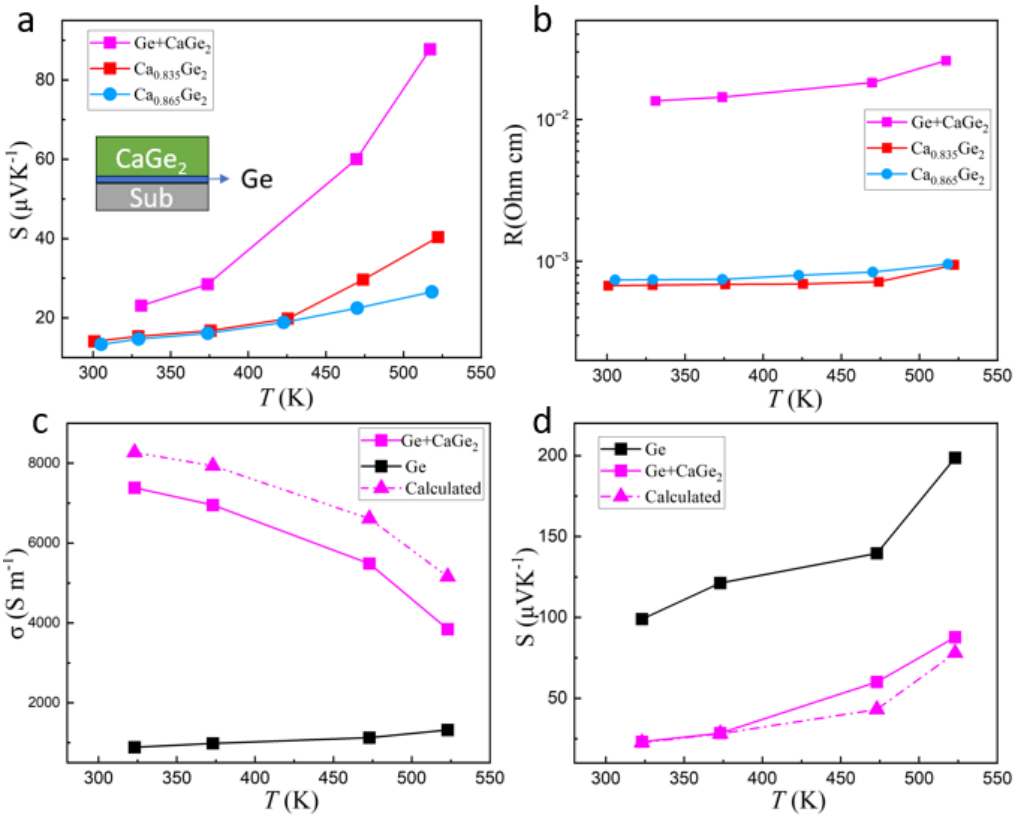

FIG. 4. (a) Temperature-dependent Seebeck coefficient of the composite film, the inset shows the structure of the composite film, and properties of $Ca_{0.835}Ge_2$ and $Ca_{0.865}Ge_2$ are also plotted for comparison; (b) resistivity R; (c)The conductivity of Ge film and composite film used as parallel conduction model calculation and (d) Calculation result of the hetero-structured film by using the parallel conduction model.

The temperature dependence of Seebeck coefficient of the hetero-structured film is shown in Fig 4 a. Due to the addition of the Ge layer, a linearly increasing Seebeck coefficient is observed, which is expected for highly doped semiconductors. This improvement in the Seebeck coefficient is regarded as the cumulative result of the thermoelectric contributions from both the upper $CaGe_2$ film and the lower Ge layer. To prove this assumption, a simple parallel conduction model is introduced to calculate the Seebeck coefficient jointly contributed by the bilayer thin films [42].

$$S = S_f + \frac{\sigma_{Ge}}{\sigma_{Ge} + \sigma_f}(S_{Ge} - S_f)$$

In the equation, S_f, σ_f, S_{Ge}, and σ_{Ge} are the Seebeck coefficient and electric conductivity of the $CaGe_2$ and Ge films, respectively, measured from thin films deposited directly onto the sapphire substrate (Figs. 3b, 3c, 4c, and 4d). The calculated results are shown in Fig. 4d, where the solid line is experimental data and the dotted line is calculated data. Near room temperature, the computed results well align with the Seebeck coefficient of the composite film. However, after 450K, the abnormal increase in the Seebeck coefficient of the film leads to a deviation from the calculated results. This phenomenon is similar to that observed in calcium-deficient films. Considering the diffusion of calcium atoms between the Ge and $CaGe_2$ layers at 600□ , a calcium-deficient Ca_xGe_2 film may form on the germanium layer. Since this abnormal increase only happens above 450K, an energy-filtering effect should not be considered because it is not sensitive

to temperature. This result suggests that the abnormal increase in the Seebeck coefficient is not caused by parallel conduction in the layers, but rather is related to the formation of a Ca deficient phase due to excess germanium and enhanced movement of Ca atom at high temperatures [44].

To summarize, this work fabricated a series of Ca_xGe_2 films on the sapphire substrate using molecular beam epitaxy method. The deficiency of Ca during deposition was found to significantly improve the crystal quality of the film. The thermoelectric properties of Ca_xGe_2 were elucidated. The $CaGe_2$ film exhibits a metallic thermoelectric behavior while the partial lack of Ca in $CaGe_2$ film effectively suppresses the bipolar effect leading to enhancement of both the Seebeck coefficient and the electric conductivity. A maximum power factor of 170 $\mu W/mK^2$ at 523 K was achieved in the $Ca_{0.835}Ge_2$ film, which is 7 times larger than the stoichiometric $CaGe_2$ film. This work highlights the significant impact of interlayer atomic modulation on the electrical transport properties in layered 2D materials.

DECLARATION OF COMPETING INTEREST

The authors declare no conflict of interest.

ACKNOWLEDGMENT

This work was supported by JST Mirai Program Grant Number JPMJMI19A1. Center support from JSPS WPI Academy is also thanked.

REFERENCE

1. Daniel Champier. Thermoelectric generators: A review of applications. Energy Conversion and Management 240, 167-181(2017).
2. Jian He and Terry M, Tritt. Advances in thermoelectric materials research: Looking back and moving forward. Science 357, 6358, eaak9997(2017).
3. Hendricks, T., Caillat, T. & Mori, T. Keynote Review of Latest Advances in Thermoelectric Generation Materials, Devices, and Technologies 2022. *Energies* vol. 15 Preprint at https://doi.org/10.3390/en15197307 (2022).
4. Petsagkourakis, I., Tybrandt, K., Crispin, X., Ohkubo, I., Satoh, N., & Mori, T. (2018). Thermoelectric materials and applications for energy harvesting power generation. *Science and technology of advanced materials*, *19*(1), 836-862.
5. Ohkubo, I., Murata, M., Lima, M. S., Sakurai, T., Sugai, Y., Ohi, A., ... & Mori, T. (2022). Miniaturized in-plane π-type thermoelectric device composed of a II–IV semiconductor thin film prepared by microfabrication. *Materials Today Energy*, *28*, 101075.
6. Seyed Mohsen Pourkiaei, Mohammad Hossein Ahmadi, Milad Sadeghzadeh, Soroush Moosavi, Fathollah Pourfayaz, Lingen Chen, Mohammad Arab Pour Yazdi, Ravinder Kumar.Thermoelectric cooler and thermoelectric generator devices: A review of present and potential applications, modeling and materials. Energy, 186, 115849 (2019).
7. X. Z. Wu, Z. Han, Y. Zhu, et al., An Engineering Roadmap for the Thermoelectric Interface Materials, *J. Materiomics,* (2023) 2300436
8. He R, Schierning G, Nielsch K. Thermoelectric devices: a review of devices, architectures, and contact optimization. Advanced Materials Technologies, 3(4): 1700256 (2018).
9. T. Mori. Novel Principles and Nanostructuring Methods for Enhanced Thermoelectrics. *Small* 13, 1702013(2017).
10. Seebeck T. J. Magnetische polarisation der metalle und erze durch temperatur-differenz. Wiss. Berlin, 289-346, (1822).
11. Snyder G. J, Snyder A. H. Figure of merit ZT of a thermoelectric device defined from materials properties. Energy & Environmental Science, 10(11): 2280-2283 (2017).
12. Pei, J., Cai, B., Zhuang, H. L., and Li, J. F. Bi2Te3-based applied thermoelectric materials: Research advances and new challenges. National Science Review (Vol. 7, Issue 12, pp. 1856–1858) (2020).
13. Heremans J P, Jovovic V, Toberer E S, et al. Enhancement of thermoelectric efficiency in PbTe by distortion of the electronic density of states. Science, 2008, 321(5888): 554-557.
14. Liu, C., Zhang, Z., Peng, Y., Li, F., Miao, L., Nishibori, E., ... & Mori, T. (2023). Charge transfer engineering to achieve extraordinary power generation in GeTe-based thermoelectric materials. *Science Advances*, *9*(17), eadh0713.
15. Wang L, Fang S, Li J, et al. Anomalous enhancement of thermoelectric performance in GeTe with specific interaxial angle and atomic displacement synergy. Cell Reports Physical Science, 2022, 3(9).
16. Dismukes, J. P., Ekstrom, L., Steigmeier, E. F., Kudman, I., & Beers, D. S. (1964). Thermal and

electrical properties of heavily doped Ge-Si alloys up to 1300 K. *Journal of Applied Physics*, *35*(10), 2899-2907.
17. Basu R, Singh A. High temperature Si–Ge alloy towards thermoelectric applications: A comprehensive review. Materials Today Physics, 21: 100468 (2021).
18. Slack G A, Hussain M A. The maximum possible conversion efficiency of silicon-germanium thermoelectric generators. Journal of applied physics, 70(5): 2694-2718 (1991).
19. Bathula S, Jayasimhadri M, Singh N, et al. Enhanced thermoelectric figure-of-merit in spark plasma sintered nanostructured n-type SiGe alloys. Applied Physics Letters, 101.21 (2012).
20. Liu W, Tan X, Yin K, et al. Convergence of conduction bands as a means of enhancing thermoelectric performance of n-type Mg 2 Si 1− x Sn x solid solutions. Physical review letters, 108(16): 166601 (2012).
21. Ahmed, F., Valenta, J., Tsujii, N., Hussain, A., Jabeen, N., & Mori, T. (2021). The low and high temperature thermoelectric properties of Yb3Si5. *Materials Research Express*, *8*(7), 075504.
22. Nozariasbmarz A, Agarwal A, Coutant Z A, et al. Thermoelectric silicides: A review. Japanese Journal of Applied Physics, 56(5S1): 05DA04 (2017).
23. Kim G, Shin H, Lee J, et al. A review on silicide-based materials: thermoelectric and mechanical properties. Metals and Materials International, 27: 2205-2219 (2021).
24. Markov M, Rezaei S E, Sadeghi S N, et al. Thermoelectric properties of semimetals. Physical Review Materials, 2019, 3(9): 095401.
25. Garmroudi, F., Parzer, M., Riss, A., Bourgès, C., Khmelevskyi, S., Mori, T., ... & Pustogow, A. (2023). High thermoelectric performance in metallic NiAu alloys via interband scattering. *Science Advances*, *9*(37), eadj1611.
26. Riss, A., Garmroudi, F., Parzer, M., Eisenmenger-Sittner, C., Pustogow, A., Mori, T., & Bauer, E. (2024). Material-efficient preparation and thermoelectric properties of metallic Ni x Au 1− x films with large power factor. *Physical Review Materials*, *8*(9), 095403.
27. Markov M, Rezaei S E, Sadeghi S N, et al. Thermoelectric properties of semimetals. Physical Review Materials, 2019, 3(9): 095401.
28. Völkl T, Aharon-Steinberg A, Holder T, et al. Demonstration and imaging of cryogenic magneto-thermoelectric cooling in a van der Waals semimetal. Nature Physics, 2024: 1-8.
29. Pan Y, Fan F R, Hong X, et al. Thermoelectric properties of novel semimetals: A case study of YbMnSb2. Advanced Materials, 2021, 33(7): 2003168.
30. Xie S, Liu W, Wan X, et al. Rational manipulation of epitaxial strains enabled valence band convergence and high thermoelectric performances in Mg3Sb2 film. Advanced Functional Materials, 2023, 33(19): 2300154.
31. Cheng R, Ge H, Huang S, et al. Unraveling electronic origins for boosting thermoelectric performance of p-type (Bi, Sb) 2Te3. Science Advances, 2024, 10(21): eadn9959.
32. Parfenov O E, Averyanov D V, Tokmachev A M, et al. High-Mobility Carriers in Germanene Derivatives. Advanced Functional Materials, 2020, 30(27): 1910643.
33. Ni Z, Liu Q, Tang K, et al. Tunable bandgap in silicene and germanene. Nano letters, 12(1): 113-118 (2012).
34. Wang Y, Ji W, Zhang C, et al. Enhanced band gap opening in germanene by organic molecule adsorption. Materials Chemistry and Physics, 173: 379-384 (2016).
35. Terada T, Uematsu Y, Ishibe T, et al. Giant Enhancement of Seebeck Coefficient by Deformation of Silicene Buckled Structure in Calcium-Intercalated Layered Silicene Film. Advanced

Materials Interfaces, 9(1): 2101752 (2022).
36. Terada T, Ishibe T, Katayama T, et al. Thermoelectric power factor enhancement of calcium-intercalated layered silicene by introducing metastable phase. Applied Physics Express, 14(11): 115505 (2021).
37. Yaokawa R, Nagoya A, Mukai K, et al. Crystal structures and thermodynamic stabilities of two new CaGe2 polymorphs. Acta Materialia, 151: 347-355 (2018).
38. Tobash P H, Bobev S. Synthesis, structure and electronic structure of a new polymorph of CaGe2. Journal of Solid State Chemistry, 180(5): 1575-1581 (2007).
39. Wangila E, Saha S K, Kumar R, et al. Single crystalline Ge thin film growth on c-plane sapphire substrates by molecular beam epitaxy (MBE). CrystEngComm, 24(24): 4372-4380 (2022).
40. Quinn R J, Bos J W G. Promising thermoelectric performance in CaAgP with intrinsic Ag vacancies. Applied Physics Letters, 120.7 (2022).
41. Markov M, Rezaei S E, Sadeghi S N, et al. Thermoelectric properties of semimetals. Physical Review Materials, 3(9): 095401 (2019).
42. Gayner C, Amouyal Y. Energy filtering of charge carriers: current trends, challenges, and prospects for thermoelectric materials. Advanced Functional Materials, 2020, 30(18): 1901789.
43. Alvarez-Quintana J. Impact of the substrate on the efficiency of thin film thermoelectric technology. Applied Thermal Engineering, 84: 206-210 (2015).
44. Kotsakidis J C, Grubišić-Čabo A, Yin Y, et al. Freestanding n-Doped Graphene via Intercalation of Calcium and Magnesium into the Buffer Layer–SiC (0001) Interface. Chemistry of Materials, 32(15): 6464-6482 (2020).